Causes for increased flood frequency in central Europe in the 19th century

Stefan Brönnimann,[1,2,*] Luca Frigerio,[1,2] Mikhaël Schwander,[1,2,3] Marco Rohrer,[1,2] Peter Stucki,[1,2] Jörg Franke[1,2]

[1] Oeschger Centre for Climate Change Research, University of Bern, Switzerland

[2] Institute of Geography, University of Bern, Switzerland

[3] Federal Office of Meteorology and Climatology MeteoSwiss

** correspondence to: stefan.broennimann@giub.unibe.ch*

Abstract

Historians and historical climatologists have long pointed to an increased flood frequency in Central Europe in the mid and late 19th century. However, the causes have remained unclear. Here, we investigate the changes in flood frequency in Switzerland based on long time series of discharge and lake levels, of precipitation and weather types, and based on climate model simulations, focusing on the warm season. Annual series of peak discharge or maximum lake level, in agreement with previous studies, display increased frequency of floods in the mid 19th century and decreased frequency after the Second World War. Annual series of warm-season mean precipitation and high percentiles of 3-day precipitation totals (partly) reflect these changes. A daily weather type classification since 1763 is used to construct flood probability indices for the catchments of the Rhine in Basel and the outflow of Lake Lugano, Ponte Tresa. The indices indicate an increased frequency of flood-prone weather types in the mid 19th century and a decreased frequency in the post-war period, consistent with a climate reconstruction that shows increased (decreased) cyclonic flow over Western Europe in the former (latter) period. To assess the driving factors of the detected circulation changes, we analyse weather types and precipitation in a large ensemble of atmospheric model simulations driven with observed sea-surface temperatures. In the simulations, we do not find an increase in flood-prone weather types in the Rhine catchment in the 19th century, but a decrease in the post-war period that could have been related to sea-surface temperature anomalies.

1. Introduction

Floods are some of the costliest natural hazards in Europe (EEA, 2018). In typical pluvio-nival river regimes in Central Europe, floods are often triggered by one or several days of heavy precipitation, but some rivers also exhibit winter floods due to longer periods of large-scale precipitation or spring floods due to heavy precipitation, amplified by snow melt. Such factors might change in the future. For instance, heavy precipitation events will become more

intense in the future according to global climate model simulations (Fischer and Knutti, 2016). An intensification of heavy precipitation events is also found in regional model simulations for Europe north of the Mediterranean (Rajczak and Schär, 2017). With increasing temperature, snow melt occurs earlier in the year, changing river regimes. Furthermore, also precipitation extremes might shift seasonally (Brönnimann et al., 2018; Marelle et al., 2018). While changes in seasonality have been found for European floods (Blöschl et al., 2017), no general increase in flood frequency has so far been detected (Madsen et al., 2014). However, past records suggest that there is considerable decadal variation in flood frequency (e.g., Sturm et al., 2001; Wanner et al., 2004; Glaser et al., 2010). It is reasonable to assume that such variations will continue into the future. In this paper we focus on decadal variability during the past 200 years.

An increased flood frequency in the 19th century was already perceived by contemporary scientists across central Europe and affected the political debates on deforestation as a potential cause (e.g., Brückner, 1990). The changing frequencies of flood events in Central Europe over the past centuries have been analysed in detail during the past 20 years (e.g., Mudelsee et al., 2004; Glaser et al., 2010). One result is that different river basins behave differently due to different hydrological regimes and different seasonality of floods. For instance, Glaser et al. (2010) found a prominent phase of increased flood frequency in central European rivers from 1780 to 1840, but mainly in winter and spring. This may not apply to Alpine rivers, which are more prone to floods in summer and autumn. Periods of increased flood frequency have also been analysed with respect to reconstructions of atmospheric circulation (e.g., Jacobeit et al., 2003; Mudelsee et al., 2004). Jacobeit et al. (2003) find that the large-scale zonal mode, which characterizes flood events in the 20th century, does not similarly characterize flood-rich periods during the Little Ice Age (their analysis, however, does not cover the 19th century). For summer floods, Mudelsee et al. (2004) find a weak but significant relation to meridional airflow. Quinn and Wilby (2013) were able to reconstruct large-scale flood risk in Britain from a series of daily weather types back to 1871 and found decadal scale changes in circulation types.

For several catchments in the Alps and central Europe, studies have suggested an increased frequency of flood events in the mid 19th century (Pfister 1984, 1999, 2009; Stucki and Luterbacher, 2010; Schmocker-Fakel and Naef, 2010a,b; Wetter et al., 2011). However, the causes of this increased flood frequency remain unclear. Besides human interventions such as deforestation or undesigned effects from water flow regulations (Pfister and Brändli, 1999; Summermatter, 2005), this includes the role of cold or warm periods and changes in

atmospheric circulation. Proxy-based studies, though focussing on longer time scales, find that in the Alps, cold periods were mostly more flood prone than warm periods (Stewart et al., 2011; Glur et al., 2013); the last of these cold and flood prone periods in the latter study is the 19th century. Glur et al. (2013) relate periods of increased flood frequency in the past 2500 years to periods of a weak and southward shifted Azores High. Even more remote factors could have played a role. Using climate model simulations, Bichet et al. (2014) investigated the roles of aerosols and of remote Pacific influences on precipitation, albeit focusing on the seasonal mean. Finally, Stucki et al. (2012) performed case studies of the strongest 24 flood events of the last 160 years. They characterised five flood-conducing weather patterns, although each extreme event had its individual combination of contributing factors.

In our paper, we aim to combine analyses of daily weather, reconstructions, and climate model simulations to elucidate potential causes leading to an increased flood frequency in Switzerland. While previous studies have focused on monthly or seasonal reconstructions, or on individual cases, we study the daily weather back to the 18th century in a statistical manner, thus bridging the gap between event analyses and paleo-climatological studies.

In this study we track the flood-frequency signal from historian documents to observations and simulations. Using long data series on floods (discharge and lake level), precipitation, daily weather types, and climate model simulations, we investigate whether an increased frequency of flood events was due to a change in seasonal mean or extreme precipitation and whether this can be related to change in weather conditions. We also address the underlying hydro-meteorological and climatological causes in model simulations. The paper is organised as follows. Section 2 describes the data and methods used. Section 3 describes the results. A discussion is provided in Section 4. Conclusions are drawn in Section 5.

2. Data and Methods

2.1. Discharge data

For the analysis of the flood frequency, we used annual peak discharge measurements from Basel, Switzerland, since 1808 (Wetter et al., 2011) as well as annual peak lake level data for Lake Constance, Constance (since 1817, supplied by the German Landesanstalt für Umwelt, Messungen und Naturschutz Baden-Württemberg) and Lago Maggiore, Locarno (Locarno (Swiss Federal Office for the Environment FOEN) since 1868. The Lago Maggiore data were corroborated by instrumental measurements at Sesto Calende for past floods since 1829 (Di Bella, 2005) and by reconstructed lake levels for floods prior to that time both for Locarno

and Sesto Calende (Stucki and Luterbacher, 2010). Further, we used a daily discharge time series for Basel and Ponte Tresa, Ticino, since 1901 from the FOEN. Figure 1 gives an overview of the catchments and locations used in this paper; Figure 2 shows the series.

Some of the series have potential inhomogeneities. Major corrections in the catchments or lakes were carried out in 1877 (Jura Waters correction, affecting the Aare and thus the Rhine), between 1888 and 1912 (Ticino in the Magadino plain), and 1943 (regulation of the level of Lago Maggiore). Lake Constance was and still is unregulated, but Jöhnk et al. (2004) argue that the level decreased by 15 cm between 1940 and 1999 due to upstream reservoirs. Based on model simulations, Wetter et al. (2011) estimate that the Jura Waters correction led to a reduction of peak discharges in Basel by 500 to 630 m^3/s. A further possible inhomogeneity concerns the level of Lago Maggiore. The flood of 1868 reportedly has led to erosion at the outflow, lowering the peak lake levels after the event. We will address these issues in Sect. 3. Note that in terms of underlying processes, lake floods slightly differ from river floods. They depend on the antecedent lake level, which carries a longer memory with it.

2.2. Precipitation data

Unfortunately, hardly any daily precipitation series covers the entire, approx. 200- year period considered here. The only long series in Switzerland is from Geneva (Füllemann et al., 2011), with daily precipitation data reaching back to 1796. Note that this series has not been homogenized prior to 1864, and that it might not be representative for the northern side of the Alps. Much more daily records exist from Switzerland from 1864 onward, the start of the Swiss network. We use data for Lugano (Ponte Tresa catchment), as well as from a number of other stations (Affoltern, Basel, Altstätten, Bellinzona, Lohn, Engelberg, see Fig. 1). Monthly precipitation was taken from the gridded HISTALP data set (Hiebl et al., 2009).

Earlier studies (e.g., Glaser et al., 2010; Stucki et al., 2012) indicate that in the region of interest, most floods occur in the warm season (hereafter May to October). The only notable exception is the Christmas flood of 1882 (marked by a star in Fig. 2). In this paper, we therefore show the results only for the warm season. From both daily precipitation series we calculate the maximum precipitation amount over 3 days per warm season, denoted Rx3day. From the gridded HISTALP data set we calculated warm season precipitation averages for two regions (Fig. 1): A region north [46.5-47.5°N, 6.5-10°E] and a region south [45.75-46.25°N, 8.5-9.25°E] of the Alpine divide.

2.3. Weather type reconstruction

In order to address flood-inducing weather patterns, we use the daily weather type reconstruction for Switzerland by Schwander et al. (2017), which reaches as far back as 1763. The weather types used in this paper are an extension of the CAP9 weather types of MeteoSwiss (Weusthoff, 2011) into the past, using station data and classifying each day according to its Mahalanobis distance from the centroids of the weather types in the calibration period. However, as two of the types were not well discernible from two other types, the respective types were merged such that only seven types remain (CAP7, see Schwander et al., 2017). This assures a good quality of the reconstruction. After 1810, the probability of each day to be attributed to the right class is higher than 80%, after 1860 it is higher than 85% (see Schwander et al. 2017). Figure 3 shows the averages of sea-level pressure per CAP7 weather type.

2.3. Reanalyses

To corroborate our results, we also consulted the "Twentieth Century Reanalysis" version 2c (20CRv2c, Compo et al. 2011). Specifically, we used daily data of precipitation, precipitable water (PWAT), and *u* wind at 850 hPa for the grid point 6°E/48°N, representing the Basel catchment. From these data we calculated Rx3d as well as a u_{850hPa}*PWAT as a measure of moisture transport from the west towards the Alps. This is important as so-called "atmospheric rivers" are important precursors to Alpine flood events (Froidevaux and Martius, 2016). We also calculated CAP7 weather types from 20CRv2c as described in Rohrer et al. (2018). In brief, we attributed each day to the closest circulation type centroid according to its Euclidian distance. Centroid were defined in the 1957-2010 based on the MeteoSwiss classification (Weusthoff, 2011). Note that all calculation were performed for each of the 56 members of 20CRv2c individually.

2.5. Climate model simulations and reconstructions

For the analysis of atmospheric circulation during the 19th and 20th century, we use the reconstruction EKF400 (Reconstruction by Ensemble Kalman Fitting over 400 years, Franke et al., 2017). This global, three-dimensional reconstruction is based on an off-line data assimilation approach of early instrumental, documentary and proxy data into an ensemble of climate model simulations. It provides an ensemble of 30 monthly reconstructions back to

1600. Here we use the ensemble mean and analyse geopotential height (GPH) and vertical velocity at 500 hPa, wind at 850 hPa as well as precipitation.

Finally, we compare the observations-based results with a large ensemble of climate model simulations. We use a 30-member ensemble of atmospheric simulations performed with ECHAM5.4 (T63) termed CCC400 (Chemical Climate Change over 400 years), which is the set of simulations that also underlies EKF400. The simulations cover the period 1600 to 2005 and are described in Bhend et al. (2012). Their most important boundary conditions are sea-surface temperature (SST) data by Mann et al. (2009). From these SSTs we also calculated indices of the Atlantic Multidecadal Oscillation (AMO) and the Pacific Decadal Oscillation (PDO) following the definitions by Trenberth and Shea (2006) and Mantua et al. (1997), respectively (see Brönnimann, 2015, for extensive comparisons of these indices and CCC400 results). Note that in these simulations, the long-term changes in land-surface properties were misspecified. We therefore performed an additional simulation with corrected land surface to assess the impacts (Rohrer et al., 2018). While no impacts were found in heavy precipitation and weather types, warm-season average precipitation showed a too strong drying trend, which we adjusted to match that of the corrected simulation. In any case, the discrepancy concerns the long-term change and not decadal-to-multidecadal variability.

Similar as for 20CRv2c, we use daily precipitation representative of the Aare catchment (47.5° N/7.4° E, see Brönnimann et al., 2018) and the CAP7 weather types from CCC400. The CAP7 weather types were evaluated by Rohrer et al. (2018): Although the model shows a zonal bias (too frequent westerly types), the decadal variability of weather type frequencies within the simulations may give some indications as to possible contribution due to SST anomalies or external forcings.

2.6. Construction of a flood probability index

From the weather types described above, we construct a flood probability index (FPI) for each river catchment following the basic methodology of Quinn and Wilby (2013). The FPI weighs the frequency of weather types according to their flood-proneness. To determine the weights, we used daily discharge data during the period 1901-2009 for Basel and Ponte Tresa. Flood events were defined using a peak-over-threshold approach. The 98th percentile of warm season days was taken as a threshold, and a declustering was applied by combining events with a maximum distance of 3 days. Compositing the events around the day of maximum discharge showed enhanced discharge already several days prior to the event. Therefore, we

199 also considered weather types on the five days prior to the event (Froidevaux (2014),
200 analysing the role of antecedent precipitation for floods in Swiss rivers, find a somewhat
201 shorter interval, but analysed smaller catchments). In the following we analyse the weather
202 types during on flood events and the preceding 7 days.

203 Figure 4 (top) shows the frequency of weather types during all warm season days for the
204 period 1901-2000. The types „northeast, indifferent“ and „west-southwest, cyclonic“, and
205 „east, indifferent“ make up 60% of all days. The most rare weather type „high pressure“
206 accounts for 5% of all days. The middle and bottom panels show the fraction of flood events
207 per weather type for Basel and Ponte Tresa (dividing the fractions in the bottom panels series
208 by the frequencies in the top panel yields w_{tl}). Of all flood days in Basel, 60% are either
209 „northeast indifferent“ or „north cyclonic“ types. The two days prior to the event are
210 dominated (77%) by the three ”cyclonic“ types, and an increase of cyclonic types is even
211 found five days ahead of the flood event (65% versus 42% on average). For Ponte Tresa, type
212 7 („westerly over southern Europe, cyclonic“) is the most flood prone, followed by „west-
213 southwest cyclonic“. The former dominates particularly one to five days ahead of the event.
214 On these days, type 7 is 4 times more frequent than on average.

215 A seasonal or annual flood probability index FPI_y can be defined in the following way. For all
216 event days in our calibration period 1901-2009 (and similarly for preceding days, l indicates
217 the lag and ranges from -5 to 0), we analysed the absolute frequency of a given weather type t
218 (n_t) relative to all event days (n_l) and divided this by the absolute frequency of that weather
219 type on all days (n_t). This ratio was termed w_{tl}:

220 $$w_{tl} = \frac{n_{tl}/n_l}{n_t} \quad (1)$$

221 To determine the *FPI* for a given year y (in our case, a warm season) we analysed the absolute
222 weather type frequencies in that year (warm season), n_{ty}, and multiplied it with the
223 corresponding weights w_{tl} for a given lag l. This results in one time series for each lag l. The
224 four series were then combined to provide the index FPI_y using a weighted average with
225 weights v_l:

226 $$FPI_y = \sum_l v_l \sum_t n_{ty} w_{tl} \quad (2)$$

227 Based on the results of Figure 4, the weights (v_l) for days -5 to 0 were set to 1/16, 1/8, 1/4,
228 1/4, and 1/8, respectively (assigning equal weights or using a shorter window yields very
229 similar results). Note that weights were recalculated for the *FPI* from 20CRv2c.

Quinn and Wilby (2013) used annual frequencies of the weather types to define the FPI. Here we calculated a daily index FPI_d, which (unlike the annual index) takes the actual sequence of weather types into account, such as during the passage of a cyclone. Equation (2) can be used for the daily index, with the same weights v_l and w_{tl} as for FPI_y, but the frequency n_{tdl} is now either zero or one:

$$FPI_d = \sum_l v_l \sum_t n_{tdl} w_{tl} \quad (3)$$

The result is a daily index FPI_d whose warm season average is by definition equal to FPI_y, but which allows also studying other statistics. To test the daily index for the case of Basel, we studied composites of FPI_d, average daily precipitation from all sites North of the Alps (Affoltern, Altstätten, Basel, Engelberg, Geneva, and Lohn), moisture transport u_{850}*PWAT from 20CRv2c, and discharge in Basel for two types of composites: (1) for peak-over-threshold flood events and (2) for peak-over-threshold events of FPI_d (defined in the same way, i.e., as declustered 98th percentile). As expected, flood events are related to a clearly increased FPI_d (Fig. 5, left). The average reaches 1.67, which means a 67% increase in flood probability. This corresponds to the 83rd percentile of FPI_d. Moisture transport is increased (to its 75th percentile) 5 to 2 days prior to the flood event. Precipitation reaches its 97th percentile on days 1 and 2 prior to the event. The mean of the selected flood events corresponds to a quantile of 99.4%. Compositing the same variables for instances with a high FPI_d (Fig. 5, right), we find similarly high percentile (99.3%) for the mean of the selcted FPI_d events. We also find high moisture transport (79th percentile) and precipitation (89th percentile) two days ahead of the event. The FPI_d clearly captures the passage of active cycones. Discharge in Basel is also increased, but only to its 71st percentile.

Thus, the index captures flood events and also moisture transport and precipitation well, although with a high rate of „false alarms" (i.e., not all FPI_d events lead to floods). This can be expected for such a coarse classification. Classifications with more types were also reconstructed, but less skilfully and hence we prefer CAP7 (Schwander et al. 2017). Another cause are the preconditions for flood events, particularly for such a large catchment as the Rhine. Discharge in Basel is on average above its 75th percentile already a week or more prior to the event, perhaps due to the passage of previous cyclones (not captured in FPI_d). A third cause for false alarms is the different sample size of flood events (n = 110) and „FPI events" (n = 285) despite using the the same threshold and declustering. This is due to the different temporal structure of the time series. Two thirds of the FPI_d events cannot be floods even if the match was perfect.

High percentiles of FPI_d are thus not suitable for studies of interannual-to-decadal variability. Flood-conducive cyclone passages occur almost every summer and hence high percentiles of FPI_d show little interannual variability. We use the warm season 75th percentile to capture the upper part of the distribution as well as the 50th percentile and the mean (i.e., FPI_y) to capture the central tendency

3. Results

3.1. Flood frequency

To begin with, we analysed the flood series in order to test whether the reported increased flood frequency in the mid-19th century is also found in our series (Fig. 4). The first thing we note is that floods do not occur synchronously across the considered catchments. The same is true for annual peak discharge series in general, as evidenced by low Spearman correlations. For instance, the series for the Rhine in Basel is uncorrelated with the series of Lago Maggiore and only moderately (coefficient of 0.36) with the series of Lake Constance, even though the latter comprises a large sub-catchment.

Was flood frequency higher in the mid-19th century? In fact, each series exhibits prominent peaks in the 19th century, e.g., the Rhine in Basel in 1817, 1852, 1876, 1881, and 1882 (see Stucki et al., 2012), Lake Constance in 1817 (see Rössler and Brönnimann, 2018) and Lago Maggiore in 1868 (Stucki et al. 2018). However, we also note a period of low flood frequency in Basel from the 1920s to 1970s, in agreement with a low frequency of peak-over-threshold events in Basel and Ponte Tresa. For further analyses we defined the 30-yr periods with highest and lowest flood frequencies, respectively, as follows: From the annual series we defined floods as exceedances of the 95th percentile of the 1901-2000 period (dashed line). Note that even accounting for a shift of 630 m^3/s due to the Jura Waters correction would not change the selected events of the Rhine in Basel, neither would a correction for a linear 15 cm trend of Lake Constance after 1940 due to an increasing number of water reservoirs upstream (cf. Jöhnk et al., 2004). However, the inhomogeneity caused by the 1868 event might be substantial. We therefore considered pre-1868 data only qualitatively.

Counting annual floods in all series as well as counting the daily peak-over-threshold events for Basel and Ponte Tresa both yields the same 30-yr period with lowest flood frequency: 1943-1972. The period with highest flood frequency is only defined by counting annual floods. Not including pre-1868 Lago Maggiore data, the period 1847-1876 is the most flood-rich. This is further supported by the historical data for Lago Maggiore, which suggest

296 additional strong flood events in that period. However, earlier 30-yr periods might be equally
297 or even more flood-rich, according to reconstructed flood events.

298 In the following we assess differences in a variable in each period relative to a corresponding
299 climatology (a sample consisting of 30 yrs before and 30 yrs after the period to further reduce
300 the effect of centennial-scale changes) as well as between the two periods with a Wilcoxon
301 test.

302

303 *3.2. Precipitation*

304 In a second step, we analysed warm-season mean precipitation and Rx3day for the regions
305 north or south of the Alps (Figs. 6 and 7). In both regions, warm season precipitation is
306 correlated significantly (Spearman correlation of 0.45 and 0.50, respectively) with annual
307 maximum discharge, clearly indicating that the floods under study are caused by excess
308 precipitation. In both regions, precipitation was slightly above the 20th century mean (dashed)
309 during most of the 19th century and below average during the flood-poor period. The
310 difference between the flood-rich (1847-1876) and the flood-poor (1943-1972) periods is
311 significant (p-value of the Wilcoxon test: $p = 0.027$) for the Ponte Tresa catchment. For the
312 Basel catchment, both periods deviate significantly negatively from the corresponding
313 neighbouring decades ($p = 0.049$ and 0.030 for the flood-rich and flood-poor period,
314 respectively), which is unexpected for the flood-rich period. Their difference is not
315 significant.

316 Rx3day for Geneva and Lugano are shown exemplarily to assess the role of extreme
317 precipitation. For Geneva, we find two pronounced extremes (1827, 1888), both of which
318 were discussed in newspapers (NN, 1827) and thus are considered real. For both stations, the
319 decreased intensity of Rx3d in the flood-poor period relative to neighbouring decades is
320 significant ($p = 0.026$ and 0.038 for the Rhine and Ponte Tresa catchments, respectively). A
321 similar decrease at the same time is also found for other series in Switzerland (Fig. 8 shows
322 six long series). Calculating for each series the annual exceedance frequency of the 95th
323 percentile (based on the 1901-2000 interval) of Rx3d and then averaging over all 8 series
324 shown in Figs. 6 to 8, we obtain a time series of the ratio of stations exceeding their 95th
325 percentile in a given year. This series shows lower values in the 1943-1972 period than in the
326 following 30 year period and even lower than in the late 19th century.

In Section 3.1 we found clear changes in flood frequency. This section shows that at least the flood-poor period was related to a reduction in the precipitation amount and intensity of Rx3d events, while results for the flood-rich period are ambiguous.

3.3. Moisture transport

In addition, we consider moisture transport from the West towards the Alps, which we analyse in 20CRv2c for the Basel catchment. As a diagnostic we calculate, similar to Rx3d, the largest 3-day average of u_{850hPa}*PWAT per summer season. This proxy for westerly moisture transport is shown together with Rx3d and FPI_y (both also calculated from 20CRv2c) in Fig. 9. For Rx3d and FPI_y we also show the observations-based series.

Results for the flood-rich period are ambiguous, and discrepancies to the observations-based series are large in parts, as is seen in FPI_d in the 1850s and 1880s in Fig. 9. This may be explained by the fact that 20CRv2c is prone to errors in the early decades (see Rohrer et al. 2018). Agreement between observations and 20CRv2c increases after 1900. Specifically, moisture transport shows similar decadal variability as *FPI* or precipitation, with higher values prior to 1940 and lower values afterwards. Although 20CRv2c alone does not permit the interpretation of decadal changes, we note that the changes are fully consistent with those in our independent time series.

3.4. Weather and large-scale flow

In the next step step, we analyse the link of flood events to atmospheric circulation and its multidecadal changes by means of the FPI_d statistics (see Sect. 2.5). The temporal development for Basel (Fig. 6, bottom) and Ponte Tresa (Fig. 7, bottom) is similar for all indicators (mean, median or 75th percentile), and the Spearman correlations of the Basel FPI_d series with the annual maximum discharge at Basel are statistically significant (p = 0.005 to 0.014). This shows that the *FPI* is a good predictor for flood variability.

For both catchments, the indices reveal clear multidecadal variability. Indices are generally positive from the 1810s to 1900s (with a secondary maximum in the 1920s and 1930s) and negative from the 1940s to around the 2000s. Both periods are longer than those selected in our study. The differences in the FPI_d between our flood-rich and flood-poor period is significant in both catchments for all three indices (max. p-value is 0.0023). The flood-rich period does not differ significantly from the neighbouring decades (which also show high values of the FPI) in any of the indices, whereas the flood-poor period shows lower values

than the neighbouring decades (p = 0.047 and 0.067 for Basel and Ponte Tresa, respectively). From these analyses we can conclude that the change in precipitation amount and intensity found in the previous Section was related to the FPI. The flood-rich and flood-poor periods clearly differ with respect to occurrence of weather types, i.e. large-scale atmospheric flow.

Floods are extreme and thus rare events, but the causes for changes in extremes do not need to be rare. Changes in extremes may be the expression of a shift in the underlying distribution. For instance, the correlations of the 75th and 90th percentile of FPI_d with the mean are 0.92 and 0.77 for the Basel catchment and 0.95 and 0.91 for the Ponte Tresa catchment. Additionally, for the case of floods, Fig. 5 shows that preconditions (and thus the previous cyclone) matter. We therefore analyse to what extent the change in weather types is mirrored in the multi-decadal atmospheric circulation statistics.

We analysed the two periods in global climate reconstructions (EKF400), each relative to its climatology as well as the difference between the two (Fig. 10). The anomalies for the flood-rich period show clear negative GPH anomalies over western Europe and strengthened flow from the north-west. The extension of the Azores onto the European continent weakened. This pattern becomes a lot stronger and clearer when contrasting the two periods (flood-rich minus food-poor). The anomalies for the flood-poor period show strengthened high-pressure influence over Central Europe, descent, and dryness with anomalous flow from the north east.

In all, the large-scale analysis confirms the results from the *FPI*: It shows clearly that the shift in weather types was an expression of multi-decadal variability of atmospheric circulation over the full North Atlantic-European sector, consisting of a more zonal and southward-shifted circulation.

3.5. Climate model simulations

We have seen that the decadal-to-multidecadal changes in flood frequency can be related to changes in weather types, which are part of large-scale flow anomalies. In the fourth step, we analysed whether this can in turn be attributed to influences such as sea-surface temperature variability modes as depicted by atmospheric model simulations (CCC400) or whether the decadal-to-multidecadal changes are due to random, possibly atmospheric variability. Concretely, we analysed warm-season mean precipitation and Rx3d for a grid point north of the Alps and calculated FPI_d and its statistics for each member. We then averaged the results across all 30 CCC400 members (one corrupt member was excluded for FPI_y). This is meaningful because changes in the ensemble mean reflect a common signal which must be

due to the common boundary conditions of the simulation. Figure 11 shows the series in a smoothed form (31-yr moving average) for visualisation.

Indeed, we note that the agreement between modelled and observation-based FPI is not good in the 19th century; the broad 19th century peak in the observation-based FPI is missing in the model. In addition, the analysis reveals downward trends in mean precipitation (although the series is trend-corrected) as well as in Rx3d. Quantitatively, the trend in mean precipitation amounts to -1.88% per century, which is rather small (much smaller than in the observations). Due to this trend it is not surprising that significant differences in seasonal mean precipitation appear between the two periods which may be unrelated to decadal-to-multidecadal variability but rather to multi-centennial trends. Differences between the averages of the flood-rich and the flood-poor periods across the ensemble are not significant for Rx3d and around the significance limit for FPI_y (Wilcoxon test: $p = 0.043$).

In the model, the flood-rich period is not significantly different from neighbouring decades in any of the measures, but the flood-poor period appears as a potentially flood-poor period in seasonal mean precipitation and FPI_y (Wilcoxon test: $p = 0.013$ and $p = 0.004$, respectively). Only model boundary conditions can explain this, and the arguably dominant contribution is from SSTs. Among the well-known SST variability modes, it is in fact the PDO index that explains the FPI_y most successfully. However, the Spearman correlation remains low and not significant in view of the low number of degrees of freedom, even after detrending.

We infer from these analyses that our climate model simulations do not reproduce the flood-rich period, but the flood-poor period appears as a feature.

4. Discussion

While tracking the flood-frequency signal, we have found a number of links and dependencies; these are discussed in the following. For instance, previous studies found an increased flood frequency in Switzerland in the 19th century (Pfister 1984, 1999, 2009; Stucki and Luterbacher, 2010; Schmocker-Fakel and Naef, 2010a,b; Wetter et al., 2011) as well as a decrease in the mid 20th century, sometimes referred to as the „disaster gap“ (Pfister, 2009; Wetter et al., 2011). The series used in this paper confirm the general tendency. Schmocker-Fackel and Naef (2010a,b) identify 1820-1940 as a flood-rich period, while we use much a shorter period. However, our *FPI* is consistent with a longer flood-rich period around 1820-1940, i.e., the difference between 1820-1940 and 1943-1972 is also highly significant ($p < 0.00001$).

Rx3day series from Geneva and Lugano together with series from a larger number of Swiss stations confirm a multidecadal period around the 1960s with reduced intensity of Rx3d. The change in the frequency of floods, which are rare events, is related to a change in mean climate. For instance, warm season mean precipitation shows changes that are concurrent with those of flood frequency, with significant correlations. We also find consistent changes for high percentiles of the *FPI* and its mean.

Schmocker-Fackel and Näf (2010a) analysed the relation between floods and weather types for the period after 1945 and manual assignments based on weather reports before that year. Here we can make use of a new, daily 250-yr weather type reconstruction. As in Schmocker-Fackel and Näf (2010a), we find that events south of the Alps and those north of the Alps are related to slightly different weather type characteristics, although indices for both regions are highly correlated on all time scales. Our *FPI* shows clear multidecadal variability, with high values during most of the 19th century and a secondary peak in the 1920s and 1930s, and lower than average values in the post-war period. After around 1980, the FPI returned to average values. The *FPI* reflects passing cyclones, but it also captures episodes of strong moisture transport, and in fact annual 3-day maxima of moisture transport in 20CRv2c show similar multidecadal variability.

In agreement with Schmocker-Fackel and Näf (2010a,b), we find no imprint on the classical NAO pattern and also no clear weakening of the Azores high during the flood-rich period. However, we find that the extension of the Azores high onto the European continent weakened, and we find clear negative GPH anomalies over western Europe, strengthened north-westerly advection, and large-scale ascent. This indicates a more zonal, southward-shifted circulation over the North Atlantic-European sector during the flood-rich period. Opposite anomalies, i.e., positive GPH anomalies and descent, are found for the flood-poor period, which was in fact associated with heatwaves and strong droughts in Central Europe. Brugnara and Maugeri (2019), find a regime shift in total precipitation and wet-day frequency for a southern region of the Alps, and for a period after the 1940s which coincides with the flood-poor period.

The flood-poor period might carry imprints of oceanic influences. Sutton and Hodson (2005) related summer climate anomalies on both sides of the Atlantic in the wider 1931-1960 period to changes in the AMO. We do not find a significant correlation between our flood and precipitation indicators and the AMO; a possible relation to the PDO index is possible but not confirmed. The flood-poor period partly overlaps with a period of poleward displacement of the northern tropical belt, which is understood to be caused by sea-surface temperature

460 anomalies and is reproduced in climate models (Brönnimann et al., 2015). Our EKF400
461 analysis is thus consistent with the results of the latter study.

462

463 **5. Conclusions**

464 Flood frequency in Central Europe exhibits multidecadal changes, which has been
465 demonstrated based on historical records. The causes for the increased flood frequency in
466 Switzerland in the 19th century as well as for the decreased flood frequency around the mid-
467 20th century are long-standing issues. In this study we have tracked these changes from flood
468 records through precipitation records, weather type statistics and large-scale circulation
469 reconstructions all the way to oceanic influences as expressed in atmospheric model
470 simulations. The change in flood frequency is arguably the expression of changes in mean
471 climate. We attribute the changes in flood frequency to changes in mean precipitation and in
472 the intensity of Rx3d. In turn, these are related to a change in cyclonic weather types over
473 Central Europe. These changes indicate a shift in large-scale atmospheric circulation, with a
474 more zonal, southward shifted circulation during the flood-rich period relative to the flood
475 poor period. Precipitation and circulation changes are only to a small part reproduced in
476 climate model simulations driven by observed sea-surface temperatures, which points to
477 random atmospheric variability as an important and complementary cause.

478 The analyses show that decadal variability in flood frequency occurred in the past; and is
479 likely to continue into the future. Better understanding its relation to weather regimes, large-
480 scale circulation, and possibly sea-surface temperature may help to better assess seasonal
481 forecasts and projections. Finally, the study also shows that the Quinn and Wilby (2013)
482 methodology also works for flood risk in Switzerland.

483

484 *Acknowledgements:* This work was supported by Swiss National Science Foundation projects
485 RE-USE (162668), EXTRA-LARGE (143219), and CHIMES (169676), by the European
486 Commission (ERC Grant PALAEO-RA, 787574) and by the Oeschger Centre for Climate
487 Change Research. Simulations were performed at the Swiss National Supercomputing Centre
488 CSCS.

489

490 **References**

491 Bhend, J., Franke, J., Folini, D., Wild, M., and Brönnimann, S.: An ensemble-based approach to
492 climate reconstructions, Clim Past 8, 963–976, 2012.

493 Bichet, A., Folini, D., Wild, M., and Schär, C.: Enhanced Central European summer precipitation in
494 the late 19th century: a link to the Tropics, Q. J. Roy. Meteorol. Soc., 140, 111–123, 2014.
495 Blöschl, G. et al.: Changing climate shifts timing of European floods, Science, 357, 588–590, 2017.
496 Brönnimann, S.: Climatic changes since 1700. Springer, Advances in Global Change Research Vol.
497 55, xv + 360 pp., 2015.
498 Brönnimann, S., Fischer, A. M., Rozanov, E., Poli, P., Compo, G. P., Sardeshmukh, P. D.: Southward
499 shift of the Northern tropical belt from 1945 to 1980, Nat. Geosc., 8, 969-974, 2015.
500 Brönnimann, S., Rajczak, J., Fischer, E., Raible, C. C., Rohrer, M., and Schär, C.: Changing
501 seasonality of moderate and extreme precipitation events in the Alps, Nat. Haz. Earth Sys. Sci., 18,
502 2047–2056, 2018.
503 Brückner, E.: Klimaschwankungen seit 1700 nebst Bemerkungen über die Klimaschwankungen der
504 Diluvialzeit. E. D. Hölzel, Wien and Olmütz, 1890.
505 Brugnara, Y., and Maugeri, M.: Daily precipitation variability in the southern Alps since the late 19th
506 century, Int. J. Climatol. (early online), 2019.
507 Compo, G. P., Whitaker, J. S., Sardeshmukh, P. D., Matsui, N., Allan, R. J., Yin, X., Gleason, B. E.,
508 Vose, R. S., Rutledge, G., Bessemoulin, P., Brönnimann, S., Brunet, M., Crouthamel, R. I., Grant,
509 A. N., Groisman, P. Y., Jones, P. D., Kruk, M. C., Kruger, A. C., Marshall, G. J., Maugeri, M.,
510 Mok, H. Y., Nordli, O., Ross, T. F., Trigo, R. M., Wang, X. L., Woodruff, S. D., and Worley, S. J.:
511 The Twentieth Century Reanalysis Project, Q. J. Roy. Meteor. Soc., 137, 1–28,
512 https://doi.org/10.1002/qj.776, 2011.
513 Di Bella, G.: Le Piene del Ticino a Sesto Calende, Cocquio Trevisago, available at:
514 http://www.prosestocalende.it/ (last access: 21 January 2019), 2005.
515 EEA: Economic losses from climate-related extremes. Copenhagen, Denmark, 17 pp., 2018.
516 Fischer, E. M., and Knutti, R.: Observed heavy precipitation increase confirms theory and early
517 models, Nat. Clim. Ch., 6, 986-991, 2016.
518 Franke, J., Brönnimann, S., Bhend, J., and Brugnara, Y.: A monthly global paleo-reanalysis of the
519 atmosphere from 1600 to 2005 for studying past climatic variations, Sci. Data, 4, 170076, 2017.
520 Froidevaux, P.: Meteorological characterisation of floods in Switzerland. PhD Thesis, University of
521 Bern, 2014.
522 Froidevaux, P., and Martius, O.: Exceptional integrated vapour transport toward orography: an
523 important precursor to severe floods in Switzerland, Q. J. R. Meteorol. Soc., 142, 1997-2012, 2016
524 Füllemann, C., Begert, M., Croci-Maspoli, M., and Brönnimann, S.: Digitalisieren und
525 Homogenisieren von historischen Klimadaten des Swiss NBCN – Resultate aus DigiHom,
526 Arbeitsberichte der MeteoSchweiz, 236, 48 pp., 2011.
527 Glaser, R. et al.: The variability of European floods since AD 1500, Climatic Change, 101, 235–256,
528 2010.
529 Glur, L., Wirth, S. B., Büntgen, U., Gilli, A., Haug, G. H., Schär, C., Beer, J., and Anselmetti, F. S.:
530 Frequent floods in the European Alps coincide with cooler periods of the past 2500 years, Sci.
531 Rep., 3, 2770, 2013.
532 Hiebl, J., Auer, I., Böhm, R., Schöner, W., Maugeri, M., Lentini, G., Spinoni, J., Brunett, M., Nanni,
533 T., Tadic, M. P., Bihari, Z., Dolinar, M., and Müller-Westermeier, G.: A high-resolution 1961-1990
534 monthly temperature climatology for the greater Alpine region, Meteorol. Z., 18, 507-530, 2009.
535 Jacobeit, J., Glaser, R., Luterbacher, J., and Wanner, H.: Links between flood events in Central Europe
536 since AD 1500 and large-scale atmospheric circulation modes, Geophys. Res. Lett., 30, 1172-1175,
537 2003.
538 Jöhnk, K. D, Straile, D., and Ostendorp, W.: Water level variability and trends in Lake Constance in
539 the light of the 1999 centennial flood, Limnologica 34, 15-21, 2004.
540 Madsen, H., Lawrence, D., Lang, M., Martinkova, M., and Kjeldsen, T. R.: Review of trend analysis
541 and climate change projections of extreme precipitation and floods in Europe, J. Hydrol., 519,
542 3634–3650, 2014.
543 Mann, M. E., Woodruff, J. D., Donnelly, J. P., and Zhang, Z. H.: Atlantic hurricanes and climate over
544 the past 1500 years, Nature, 460, 1256–1260, 2009.

Mantua, N. J., Hare, S. R., Zhang, Y., Wallace, J. M., and Francis, R. C.: A Pacific interdecadal climate oscillation with impacts on salmon production, B. Amer. Meteorol. Soc., 78, 1069-1079, 1997.

Marelle, L., Myhre, G., Hodnebrog, Ø., Sillmann, J., and Samset, B. H.: The changing seasonality of extreme daily precipitation, Geophys. Res. Lett., 45, 11,352–11,360, 2018.

Mudelsee, M., Börngen, M., Tetzlaff, G., and Grünewald, U.: Extreme floods in central Europe over the past 500 years: Role of cyclone pathway "Zugstrasse Vb", J. Geophys. Res., 109, D23101, 2004.

NN: Sur un pluie extraordinaire tombée le 20 Mai 1827, dans la vallée du Léman. *Bibliothèque universelle,* **35,** 84.

Pfister, C.: Wetternachhersage: 500 Jahre Klimavariationen und Naturkatastrophen (1496-1995), Haupt, Bern, 1999.

Pfister, C.: Die "Katastrophenlücke" des 20. Jahrhunderts und der Verlust traditionalen Risikobewusstseins, Gaia 18, 239–246, 2009.

Pfister, C. and Brändli, D.: Rodungen im Gerbirge - Überschwemmungen im Vorland: Ein Deutungsmuster macht Karriere. In: Sieferle, R. P., and Breuninger, H. (eds) Natur-Bilder.Wahrnehmungen von Natur und Umwelt in der Geschichte, Campus Verlag, Frankfurt/Main and New York, pp. 297–323, 1999.

Pfister, C.: Das Klima der Schweiz von 1525 bis 1860 und seine Bedeutung in der Geschichte von Bevölkerung und Landwirtschaft. Paul Haupt, Bern, 184+163 pp., 1984.

Quinn, N. and Wilby, R. L.: Reconstructing multi-decadal variations in fluvial flood risk using atmospheric circulation patterns, J. Hydrol., 487. 109-121, 2013.

Rajczak, J., and Schär, C.: Projections of future precipitation extremes over Europe: A multimodel assessment of climate simulations, J. Geophys. Res., 122, 10,773–10,800, 2017.

Rohrer, M., Brönnimann, S., Martius, O., Raible, C. C., Wild, M., and Compo, G. P.: Representation of cyclones, blocking anticyclones, and circulation types in multiple reanalyses and model simulations, J. Clim., 31, 3009–3031, 2018.

Rössler, O., and Brönnimann, S.: The effect of the Tambora eruption on Swiss flood generation in 1816/1817, Sci. Tot. Env., 627, 1218-1227, 2018.

Schmocker-Fackel, P., and Naef, F.: Changes in flood frequencies in Switzerland since 1500, Hydr. Earth. Sys. Sci., 14, 1581–1594, 2010a.

Schmocker-Fackel, P., and Naef, F.: More frequent flooding? Changes in flood frequency in Switzerland since 1850, J. Hydrol., 381, 1–8, 2010b.

Schwander, M., Brönnimann, S., Delaygue, G., Rohrer, M., Auchmann, R., and Brugnara, Y.: Reconstruction of Central European daily weather types back to 176,. Int. J. Climatol., 37, 30-44, 2017.

Stewart, M. M., Grosjean, M., Kuglitsch, F. G., Nussbaumer, S. U., and von Gunten, L.: Reconstructions of late Holocene paleofloods and glacier length changes in the Upper Engadine, Switzerland (ca. 1450 BC–AD 420), Palaeogeogr. Palaeocl. Palaeoecol., 311, 215–223, 2011.

Stucki, P. and Luterbacher, J.: Niederschlags-, Temperatur- und Abflussverhältnisse der letzten Jahrhunderte, Hydrologischer Atlas der Schweiz, Tafel 1.4 (HADES 1.4), 2010.

Stucki, P., Rickli, R., Brönnimann, S., Martius, O., Wanner, H., Grebner, D., and Luterbacher, J.: Weather patterns and hydro-climatological precursors of extreme floods in Switzerland since 1868, Meteorol. Z., 21, 531-550, 2012.

Stucki, P., Bandhauer, M., Heikkilä, U., Rössler, O., Zappa, M., Pfister, L., Salvisberg, M., Froidevaux, P., Martius, O., Panziera, L., and Brönnimann, S.: Reconstruction and simulation of an extreme flood event in the Lago Maggiore catchment in 1868, Nat. Hazards Earth Syst. Sci., 18, 2717-2739, https://doi.org/10.5194/nhess-18-2717-2018, 2018.

Sturm, K., Glaser, R., Jacobeit, J., Deutsch, M., Brazdil, R., Pfister, C., Luterbacher, J., and Wanner, H.: Hochwasser in Mitteleuropa seit 1500 und ihre Beziehung zur atmosphärischen Zirkulation, Peterm. Geogr. Mitt., 145 (6), 14-23, 2001.

Summermatter, S.: Die Überschwemmungen von 1868 in der Schweiz, Verlag Traugott Baulz, 352. pp., 2005.

598 Sutton, R. T, and Hodson, D. L.: Atlantic Ocean forcing of North American and European summer
599 climate, Science, 309, 115-118, 2005.
600 Trenberth, K. E., and Shea D. J.: Atlantic hurricanes and natural variability in 2005, Geophys. Res.
601 Lett., 33, L12704, 2006.
602 Wanner, H., Beck, C., Brazdil, R., Casty, C., Deutsch, M., Glaser, R., Jacobeit, J., Luterbacher, J.,
603 Pfister, C., Pohl, S., Sturm, K., Werner, P. C., and Xoplaki, E.: Dynamic and socioeconomic
604 aspects of historical floods in Central Europe, Erdkunde, 58, 1-16, 2004.
605 Wetter, O., Pfister, C., Weingartner, R., Luterbacher, J., Reist, T., and Trösch, J.: The largest floods in
606 the High Rhine basin since 1268 assessed from documentary and instrumental evidence, Hydrol.
607 Sci. J., 56, 733–758, 2011.
608 Weusthoff, T.: Weather Type Classification at MeteoSwiss: Introduction of New Automatic
609 Classification Schemes. Bundesamt für Meteorologie und Klimatologie, MeteoSchweiz, 2011.

Figures

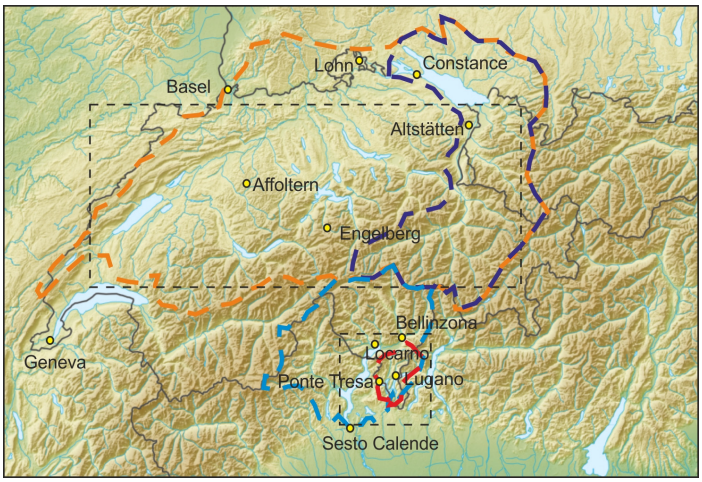

Fig. 1. Topographic map of the central Alps showing the catchments and locations mentioned in the text, the catchments of the Rhine in Basel (orange), Lake Constance (dark blue), Lago Maggiore (light blue) and Ponte Tresa (red). The rectangle boxes indicate the areas chosen for averaging precipitation in the HISTALP data.

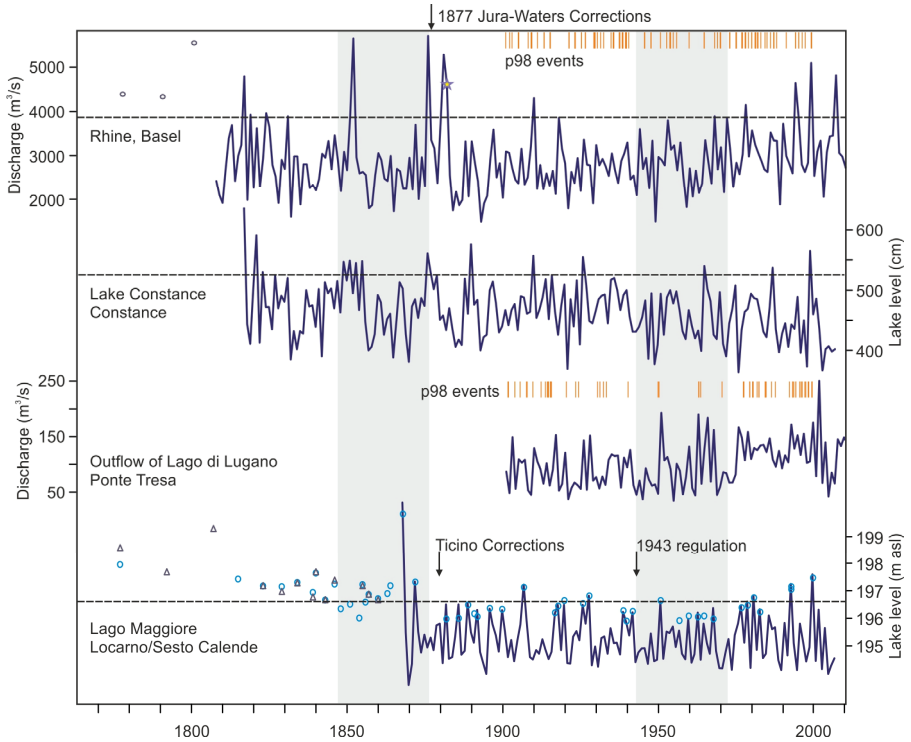

Fig. 2. Time series of annual maxima of discharge or lake level in four catchments. Symbols denote reconstructed floods based on historical sources (circles for Rhine, Basel, from Wetter et al. 2011, Triangles for Lago Maggiore, Locarno, from Stucki and Luterbacher, 2010, light blue circles for Lago Maggiore refer to floods at Sesto Calende according to Di Bella, 2005, from reconstruction prior to 1829 and measurements afterwards, adjusted to Locarno by adding the average difference between the two during floods after 1868, i.e., 0.49 m). Arrows indicate major river corrections. Orange bars indicate the peak-over threshold events in the 1901-2000 period that were used to calibrate the FPI. Grey shading denotes the flood-rich period (1847-1876) and flood-poor period (1943-1972). Dashed lines indicate the 95th percentile from 1901-2000. The star marks the Christmas flood of 1882.

626

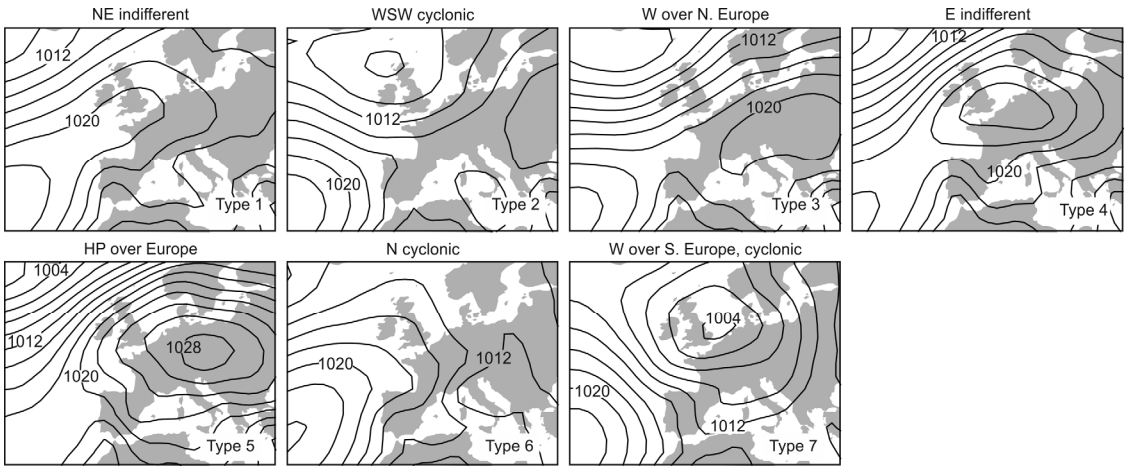

627

628 **Fig. 3.** Sea-level pressure averaged for each of the 7 weather types in CAP7 over the warm season
629 (May-Oct) for the period 1958-1998 based on 20CRv2c.

630

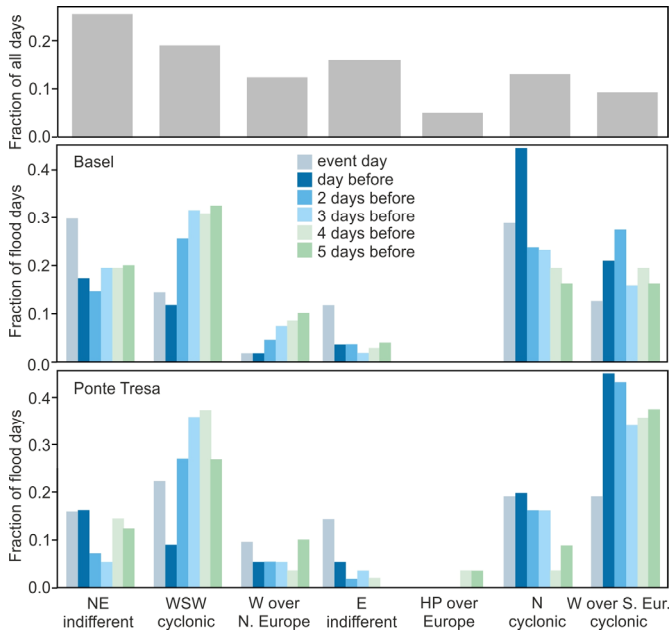

631

632 **Fig. 4.** Frequency of CAP7 weather types in the warm season (top). Fraction of flood days occurring
633 during a specific weather types for Basel (middle) and Ponte Tresa (bottom) as well as corresponding
634 series for days 1 to 5 prior to the discharge peak. The figure is based on data from 1901-2000.

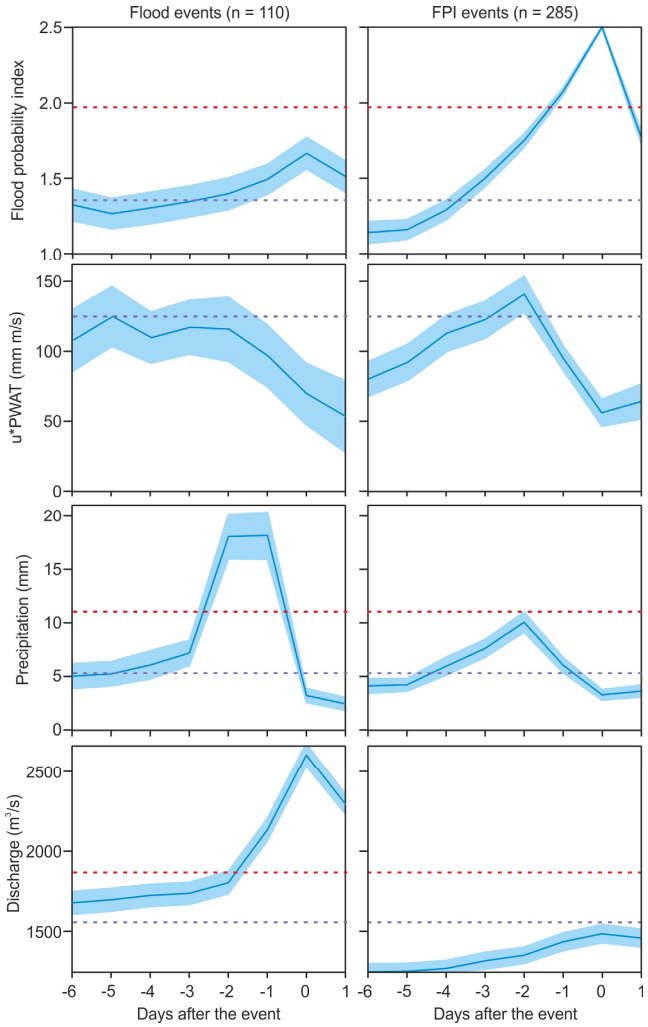

635

636 **Fig. 5.** Composites of FPI_d, u_{850hPa}*PWAT, precipitation, and discharge in Basel for (left) flood events
637 in Basel and (right) FPI_d events on 1901-2000 for 6 days preceding to 1 day following event day (day
638 0). Shading indicates two standard deviations. The red and purple dashed lines indicate the 90th and
639 75th percentile, respectively.

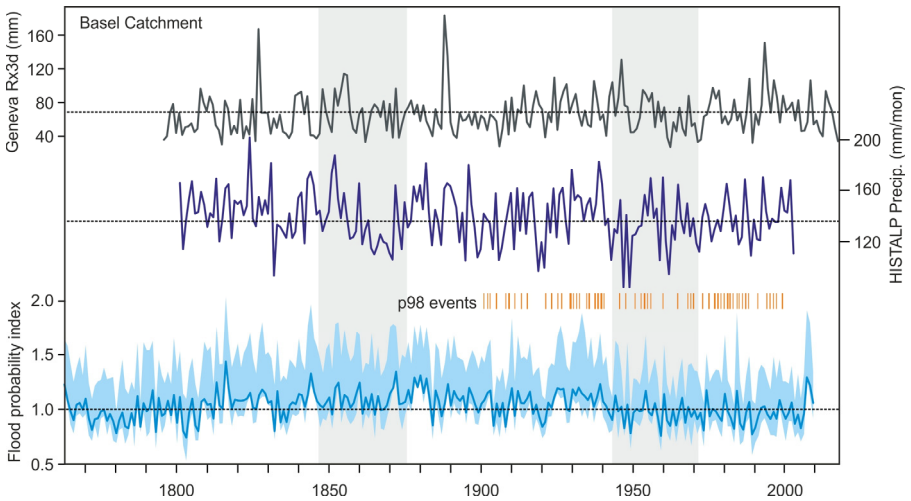

Fig. 6. Warm season Rx3d from the station Geneva (top), warm season mean precipitation in HISTALP for the Rhine catchment (middle) and flood probability index for Basel (bottom, solid indicates the warm season mean, blue shading indicates the median and 75th percentile, respectively). Dashed lines indicate the 1901-2000 average. Also shown are the peak-over threshold events (p98) of Basel discharge that were used for calibration. Grey shading denotes the flood-rich period (1847-1876) and flood-poor period (1943-1972).

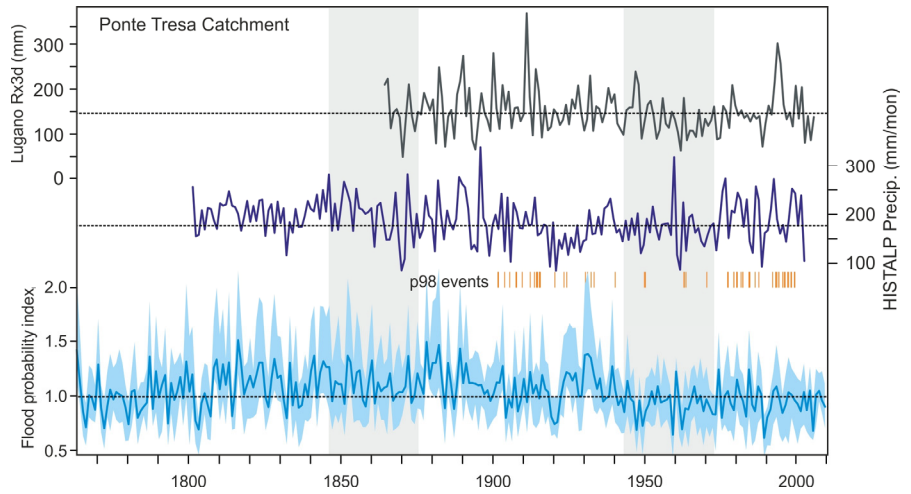

Fig. 7. Warm season Rx3d from the station Lugano (top), warm season mean precipitation in HISTALP for the Ponte Tresa catchment (middle) and flood probability index for Ponte Tresa (bottom, solid indicates the warm season mean, blue shading indicates the median and 75th percentile, respectively). Dashed lines indicate the 1901-2000 average. Also shown are the peak-over threshold events (p98) of Ponte Tresa discharge that were used for calibration. Grey shading denotes the flood-rich period (1847-1876) and flood-poor period (1943-1972).

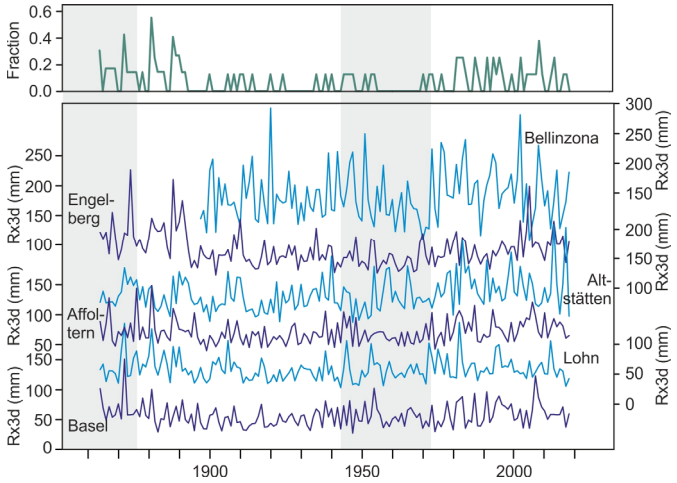

656

657 **Fig. 8.** Series of Rx3day for six further stations with long precipitation series (see Fig. 1 for locations).
658 The top line shows the fraction of these six series plus those of Lugano and Geneva shown in Figs. 5
659 and 6, exceeding their 95th percentile (based on 1901-2000) in any given year. Grey shading denotes
660 the flood-rich period (1847-1876) and flood-poor period (1943-1972).

661

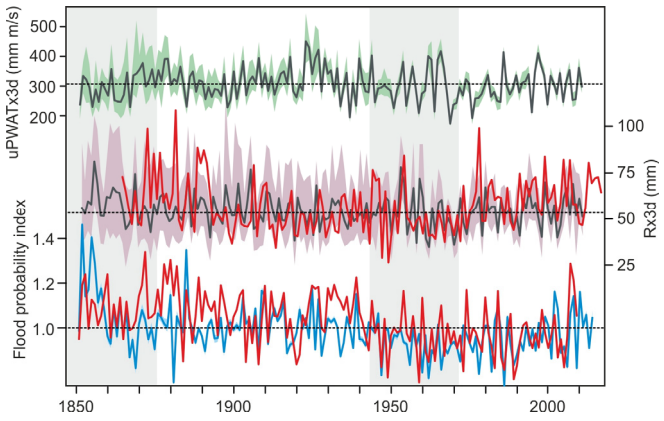

662

663 **Fig. 9.** Maximum 3-day average per warm season of (top) eastward moisture transport (u_{850hPa}*PWAT)
664 and (middle) precipitation, both at the grid point 6°E/48°N in 20CRv2c. Bottom: Warm-season mean
665 FPI index in 20CRv2c. Shading denotes the ensemble range (min. and max.). Red lines show the
666 corresponding series from observations (Rx3d is calculated form the average of all stations north of
667 the Alps). Dashed lines indicate the average value for 1901-2000 in 20CRv2c. Grey shadings denote
668 the flood-rich (1847-1876) and flood-poor (1943-1972) periods, respectively.

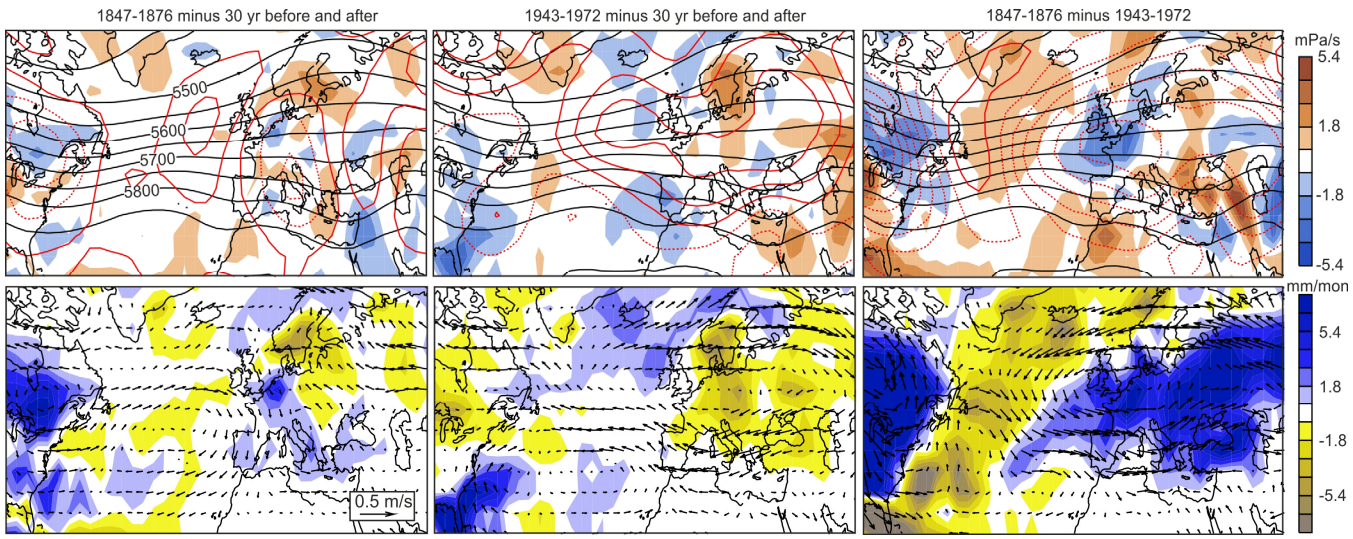

669

670 **Fig. 10.** Anomalies of (top) 500 hPa GPH (red contours, 2 gpm spacing symmetric around zero,
671 negative contours are dashed, black lines indicate the reference period average) and vertical velocity
672 (colours, lifting is blue) and (bottom) 850 hPa wind and precipitation. Shown are anomalies for the
673 1847-1876 period (left) and the 1943-1972 period (middle) with respect to the 30 yrs before and after
674 as well as (right) the difference between the two periods.

675

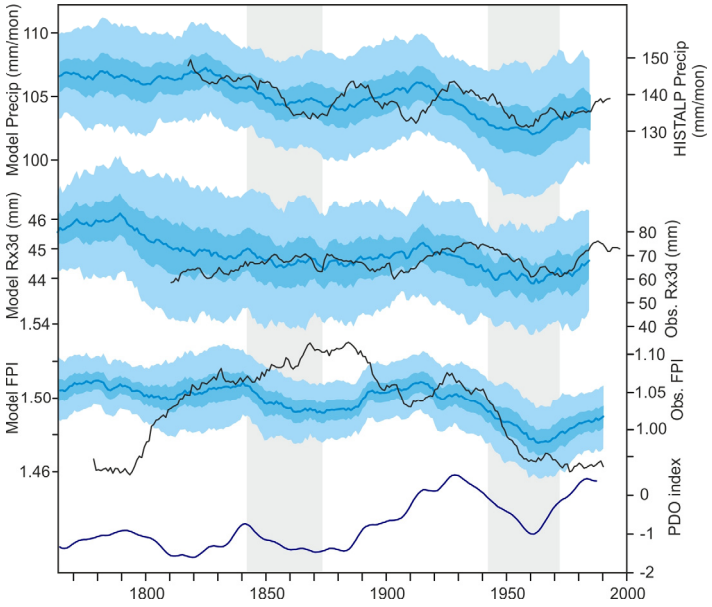

676

677 **Fig. 11.** CCC400 (left scales) warm season average precipitation (top, note that this series was
678 detrended based on the corrected member), Rx3day in the warm season at the grid point north of the
679 Alps (second from top) and flood probability index based on weather types in CCC400 (third from
680 top). The lowest line shows the PDO index in the model simulations. The solid blue lines show the
681 ensemble mean of the series smoothed with a 31-yr moving average. Light and dark shadings indicate
682 the ensemble standard deviation and the 95% confidence interval of the ensemble mean, respectively.
683 Black lines (right scales) show the corresponding observation-based series. Note the different scales.
684 Grey shadings denote the flood-rich (1847-1876) and flood-poor (1943-1972) periods, respectively.